Tunable Plasmon Induced Transparency in a Metallodielectric Grating Coupled With Graphene Metamaterials

Tian Zhang, Jian Dai, Yitang Dai, Yuting Fan, Xu Han, Jianqiang Li, *Senior Member, IEEE,*
Feifei Yin, Yue Zhou, and Kun Xu

Abstract—A novel metallodielectric grating coupled with graphene metamaterials (MGCGM) structure is proposed to achieve the tunable plasmon induced transparency (PIT) effect. Two different mechanisms are employed to explain the PIT effect in the reflection spectrum: one is originated from the destructive interference between graphene plasmonic modes and the hybrid mode in the dielectric layer, the other is related to the absorption of the graphene surface plasmons. The simulated results indicate high tunability in the amplitude and the operating wavelength of the PIT effect can be obtained by controlling the Fermi levels of graphene ribbons. Besides, double PITs are demonstrated in this scheme by altering the occupation ratio of the graphene-based ribbon grating. Compared with previous reports, the MGCGM structure is much easier to fabricate and the tunable PIT effect has significant applications in optical modulator, switching, absorber, sensor, slow light, etc.

Index Terms—Diffraction gratings, graphene, metamaterial, plasmon induced transparency (PIT).

I. INTRODUCTION

PLASMON induced transparency (PIT) effect [1], which is a plasmonic analog to the quantum electromagnetic induced transparency in atomic systems, has attracted a great deal of attention due to its abnormal dispersion and momentous applications, such as optical switching, slow light, modulator, filter, sensor, absorber and so on [2], [3]. Until now, diversified

T. Zhang, J. Dai, Y. Dai, Y. Fan, J. Li, F. Yin, and Y. Zhou are with the State Key Laboratory of Information Photonics and Optical Communications, Beijing University of Posts and Telecommunications, Beijing 100876, China (e-mail: ztian@bupt.edu.cn; daijian@bupt.edu.cn; ytdai@bupt.edu.cn; fanyuting@bupt.edu.cn; jianqiangli@bupt.edu.cn; yinfeifei@bupt.edu.cn; yuezhou@bupt.edu.cn).

X. Han is with Wuhan National Laboratory for Optoelectronics, Huazhong University of Science and Technology, Wuhan 430074, China (e-mail: hanxu567@126.com).

K. Xu is with the School of Science and State Key Laboratory of Information Photonics and Optical Communications, Beijing University of Posts and Telecommunications, Beijing 100876, China (e-mail: xukun@bupt.edu.cn).

plasmonic structures have been proposed to achieve the PIT effect, for instance, a plasmonic waveguide coupled with cavities [4], [5], metamaterials [6], [7], metallic grating coupled with dielectric waveguide layer [8], [9]. In order to find more extensive and flexible applications in reality, the tunable PIT effect, whose optical characteristics including central wavelength, amplitude and bandwidth of the transparency window could be varied with external parameters, has been extensively researched. In general, the thermally tuning method [10], [11], magnetically tuning method [12] and other tuning methods [13]–[15] have shown the potential in achieving the dynamically tunable PIT effect. For example, the tunable PIT effect has experimentally been achieved based on the thermo-optic effect, i.e., the refractive index of the PMMA coated on the plasmonic waveguide coupled with cavities changes with the temperature [11]. However, the response time of the thermally tuning method and magnetically tuning method has been demonstrated several microseconds, which limited its extensive application [10]. In order to realize the ultrafast tunability, the optical Kerr effect have been proposed to achieve the response time at the order of picosecond [16]–[18]. Nevertheless, limited by the relatively small Kerr coefficient of the adopted materials, its operating pump intensity often reaches the order of GW/cm^2 to get an ideal performance. Moreover, the precision of focused ion beam and electron beam lithography is subject to the current nanofabrication, hence the structural parameters of fabricated samples (especially for the plasmonic waveguide coupled with cavities structure) are usually different from the designed ones [19]. Obviously, it is necessary to design a plasmonic structure, which is much easier to fabricate and achieve dynamically tunable PIT effect.

In recent years, the tunable PIT effect based on graphene has attracted considerable attention due to the dynamical tunability of the graphene's conductivity by changing the Fermi energy level via chemical doping, electrostatic gating, and magnetic field [20]–[22]. For example, it has been demonstrated that the tunable PIT effect can be achieved in planar graphene metamaterials [23], [24], a graphene-based waveguide coupled cavities [25], single-layer graphene-based ribbon gratings (GRG) [26]–[28], double GRGs [29], and multilayer graphene metamaterials spatially separated by dielectric layer [30]. Although the desired PIT effect could be obtained in the above-mentioned
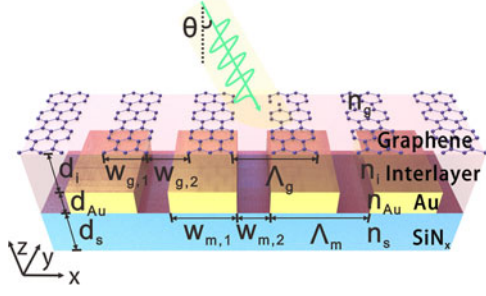
Fig. 1.   Structure schematic of the proposed MGCGM structure.

plasmonic structures, the relatively complex device design brought a great challenge in fabrication process. It is noteworthy that the excitation of the surface plasmon polaritons (SPPs) on the surface of graphene layer with low propagation loss and high confinement has been observed in a plasmonic structure composed of monolayer graphene and a silicon diffractive grating [31], [32]. Thus, it would be an efficient method to excite the SPPs on graphene layer by employing the metal diffractive grating in the metallic grating coupled with dielectric waveguide layer structure, providing a promising way to achieve a significant PIT effect. In addition, compared with the plasmonic waveguide coupled with cavities structures and planar metamaterials, the metallic grating coupled with dielectric waveguide layer structures have an ultra-narrow bandwidth and a relatively simple fabrication [33]. Clearly, it's highly expected to obtain tunable PIT effect in a graphene-assisted metallic grating coupled with dielectric waveguide layer structure with low-complexity.

Motivated by the above fundamental studies, in this paper, a metallodielectric grating coupled with graphene metamaterials (MGCGM) structure is proposed to obtain tunable PIT effect in the mid-infrared region. The destructive interference of the graphene surface plasmons (GSPs) on the GRG and the hybrid mode excited by the metal grating induces the PIT effect in the reflection spectrum of the MGCGM structure. Our calculated results reveal that the amplitude and the operating wavelength of the PIT effect can be significantly tuned by controlling the Fermi levels of the GRG. In addition, we also investigate the realization of the multi-PIT effects, slow light and refractive index sensor based on our proposed MGCGM structure.

II. DEVICE DESIGN

The proposed MGCGM structure is exhibited in Fig. 1 schematically. Obviously, the structure is free-standing and it comprises a gold film periodically pierced by narrow slits and a thin SiN_x dielectric layer. The thickness of the SiN_x layer and the grating period are fixed to be $d_s = 540$ nm and $\Lambda_m = 3800$ nm, respectively. On consideration, we select the thickness of the gold grating, the width of the gold and slit in one periodic unit as $d_{Au} = 70$ nm, $w_{m,1} = 3585$ nm and $w_{m,2} = 215$ nm, respectively, and keep them fixed in the following calculations. The frequency-dependent permittivity of gold is described by well-known Drude model $n_{Au}(\lambda) = \{1 - [(\lambda_p/\lambda + i\gamma)\lambda_p/\lambda]^{-1}\}^{1/2}$, where $\lambda_p = 160$ nm represents

the plasma wavelength and $\gamma = 0.0077$ denotes the metal loss [34]. The GRG is separated by a spacer layer with thickness $d_i = 500$ nm. Here, the graphene in GRG is modeled as an anisotropic material whose in-plane permittivity is distinct from the out-of-plane one (2.5) [35]. Its in-plane permittivity can be described as $n_g = [1 + i\sigma_g\eta_0/(k_0 d_g)]^{1/2}$, where $\eta_0 (\approx 377\,\Omega)$ and $d_g = 0.34$ nm are the impedance of air and the thickness of single-layer graphene, respectively. The surface conductivity of graphene σ_g can be retrieved by the Kubo formula based on the dyadic Green's functions [35], [36]:

$$\sigma_{g,s} = -\frac{ie^2(\omega + i\tau^{-1})}{\pi\hbar^2} \left[\int_{-\infty}^{+\infty} \frac{|\varepsilon|}{(\omega + i\tau^{-1})^2} \frac{\partial f_d(\varepsilon)}{\partial\varepsilon} d\varepsilon \right.$$
$$\left. - \int_0^{+\infty} \frac{\partial f_d(-\varepsilon) - \partial f_d(\varepsilon)}{(\omega + i\tau^{-1})^2 - 4(\varepsilon/\hbar)^2} d\varepsilon \right] \quad (1)$$

here, where $f_d = 1/(1 + \exp[(\varepsilon - E_f)/(k_B T)])$ is the Fermi-Dirac distribution, ε, E_f, $T = (300\text{ K})$, e, $\hbar$, k_B, and $\tau = (0.5\text{ ps})$ represent energy, Fermi levels, temperature, electron charge, reduced Planck's constant, Boltzmann constant, and momentum relaxation time, respectively. In the mid-infrared range where $|\mu_c| \gg k_B T$, the expression of surface conductivity can be approximated as

$$\sigma_{g,s} = i\frac{e^2 k_B T}{4\pi\hbar^2(\omega + i\tau^{-1})} \left[\frac{E_f}{k_B T} + 2\ln\left(\exp\left(-\frac{E_f}{k_B T}\right) + 1\right) \right]$$
$$+ i\frac{e^2}{4\pi\hbar} \ln\left[\frac{2|E_f| - \hbar(\omega + i\tau^{-1})}{2|E_f| + \hbar(\omega + i\tau^{-1})} \right] \quad (2)$$

where the first and second terms correspond to the intraband and interband electron-photon scattering processes, respectively. Here, the period of GRG $\Lambda_g = 380$ nm is fixed to exhibit, and the occupation ratio of graphene is set to 0.5 ($w_{g,1} = 190$ nm).

It is rather remarkable that our proposed MGCGM structure can be fabricated by current nanofabrication technology. First of all, a 540-nm-thick SiN_x layer is deposited by plasma enhanced chemical vapor deposition on a 300-μm-thick silicon substrate, followed by the deposition of silica on the other side. Secondly, the gold grating is fabricated by the use of electron beam lithography and liftoff process [34]. Thirdly, the grating is coated with the interlayer on the top of sample. Fourthly, a large window is opened in the backside silica layer and the silicon substrate is etched in tetramethyl ammonium hydroxide solution, forming a free standing SiN_x film. Fifthly, monolayer graphene grown by chemical vapour deposition is transferred to the surface of the interlayer. Then, the GRG is fabricated by using electron beam lithography followed by oxygen plasma etching [37]. Finally, Au/Cr electrodes or back-gate structures are deposited onto the GRG to control the Fermi level of the graphene ribbons grating [37].

III. CALCULATED RESULTS AND DISCUSSIONS

In order to understand the PIT effect which would occur in the designed MGCGM structure, first of all, we analyze the optical responses of the metallodielectric grating structure [Fig. 2(a)]. Here, the geometry parameters of this structure are as same
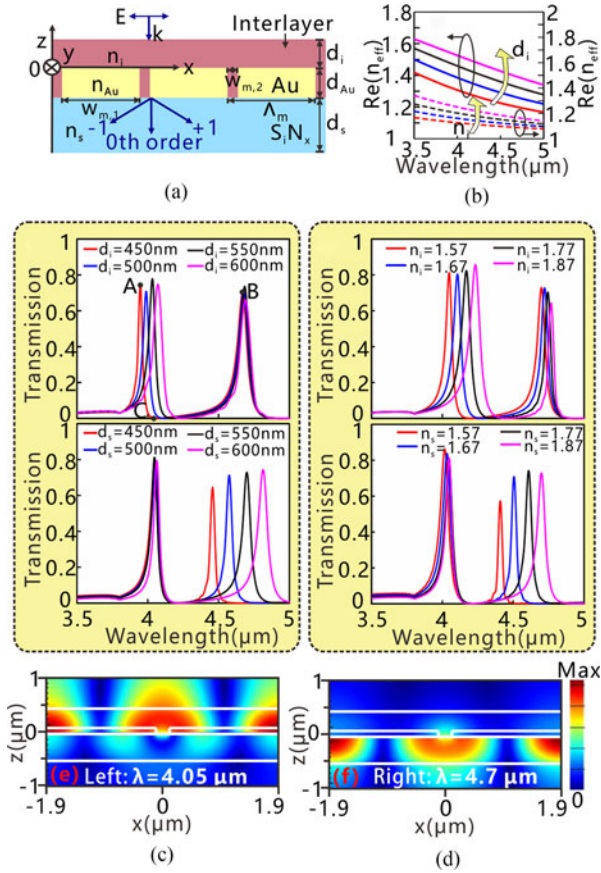
Fig. 2. (a) The schematic of the metallodielectric grating structure. (b) Dispersion curves of the fundamental hybrid mode guided in metal-dielectric-air model at different thicknesses d_i and refractive indices n_i. (c) Simulated transmission spectrum for the metallodielectric grating with different thicknesses of the interlayer (d_i, up panel) and the SiN_x dielectric layer (d_s, bottom panel). (d) Simulated transmission spectrum for the metallodielectric grating with different refractive indices of the interlayer (n_i, up panel) and the SiN_x dielectric layer (n_s, bottom panel). Spatial magnetic field distributions corresponding to transmission peaks represented by point A (e) and B (f) in (c).

as that of the above MGCGM structure. When TM-polarized plane wave normally incident onto the metallodielectric grating structure, the transmission spectrums for the structure with different geometric parameters are presented in Fig. 2(c) and (d). The characteristic spectral responses are calculated by using the finite-difference time-domain (FDTD) method (adopting the commercial software Lumerical FDTD Solutions). In our simulations, the periodic boundary conditions are used in x direction, and the other boundaries employ the perfectly matched layer boundary conditions. As shown in the up panel of Fig. 2(c), when the refractive index of interlayer (n_i) is fixed to be 1.57, we can find that two transmission peaks whose amplitude up to 79% and 72% emerge at the resonant wavelength $\lambda = 4.05$ μm and 4.71 μm, respectively. Due to the obvious asymmetry of the transmission peak A, we can conclude that the reason for the occurrence of this abnormal peak is related to the Fano resonance, which is attributed to the destructive interference between a wideband bright mode the spatial magnetic field distribution corresponding to the characteristic wavelength represented by A. Apparently, here, the wideband bright mode in the

metallodielectric grating relates to the zeroth diffracted order resonance, which can directly transmit through the gold grating; while the narrowband dark mode relates to the guide mode resonance trapping in the interlayer upon the gold grating. Nevertheless, it is rather remarkable that the reason for the occurrence of the transmission peak A is quite different from the transmission peak B. Fig. 2(f) exhibits the magnetic field distribution calculated for the peak B. It can be clearly observed that the guided mode resonance along the x direction is excited in the SiN_x dielectric waveguide layer, and the interlayer upon the gold grating don't contribute to this abnormal peak B. It should be noted that the calculated results are distinct from the results in ref. [34] where the transmission peak B related to the guide mode resonance in the SiN_x layer is no longer a Fano resonance. The reason for this phenomenon is that the appearance of the Fano resonance (peak A) leads the transmission of the dip C close to 0. Thus, the symmetrical characteristic of the peak B can be guaranteed.

It should be noted that the refractive index (thickness) of the interlayer (SiN_x dielectric layer) have a great influence on the transmission characteristics of the metallodielectric grating. In order to analysis the dispersion of the fundamental hybrid mode guided in the interlayer upon the gold grating, we regard the gold grating as a gold film for simplicity due to the quite small occupation ratio of the slits (0.05). On the other hand, the gold film is regarded as a semi-infinite thickness layer since the gold layer is thick enough to impede the penetration of light through the gold layer. Since the fundamental hybrid mode is a guided mode in this metal-dielectric-air model, we can deduce that the field in the interlayer is an oscillating field. Thus, the field in interlayer is a superposition of a sine and a cosine function, while the fields in metal and air would be an exponential function. The magnetic field in this model can be written as

$$H_y(x) = \begin{cases} A \exp(qz), & z < 0 \\ B \cos(\kappa z + \varphi), & 0 \le z < d_i \\ C \exp[-p(z - d_i)], & d_i \le z \end{cases} \quad (3)$$

where $p = k_0 (n_{eff}^2 - \varepsilon_0)^{1/2}$, $q = k_0 (n_{eff}^2 - \varepsilon_{Au})^{1/2}$, $\kappa = k_0 (n_i^2 - n_{eff}^2)^{1/2}$, and n_{eff} is the effective refractive index of the fundamental hybrid mode. Utilizing the continuous condition of H_y and $n^{-2}(dH_y/dx)$ at boundary $z = 0$ and $z = d_i$, we obtain the dispersion equation [38]

$$\kappa d_i = \arctan\left(\frac{n_i^2 p}{\varepsilon_0 \kappa}\right) + \arctan\left(\frac{n_i^2 q}{n_{Au}^2 \kappa}\right). \quad (4)$$

The calculated dispersion curves are shown in Fig. 2(b). It can be found that the real part of n_{eff} [$Re(n_{eff})$] increases with the augment of both thickness d_i and refractive index n_i of the dielectric layer, while $Re(n_{eff})$ decreases with the increasing of wavelength of incident light. Here, it's important to note that the fundamental hybrid mode can only be excited when satisfying the phase-matching condition, which can be deduced as $\lambda = n_{eff}\Lambda$ for the normally incident light at fundamental diffraction order [32]. Thus, the increasing of both d_i and n_i can leads to a red-shift of the resonant wavelength of the excited hybrid mode. As shown in Fig. 2(c), with the increase of the
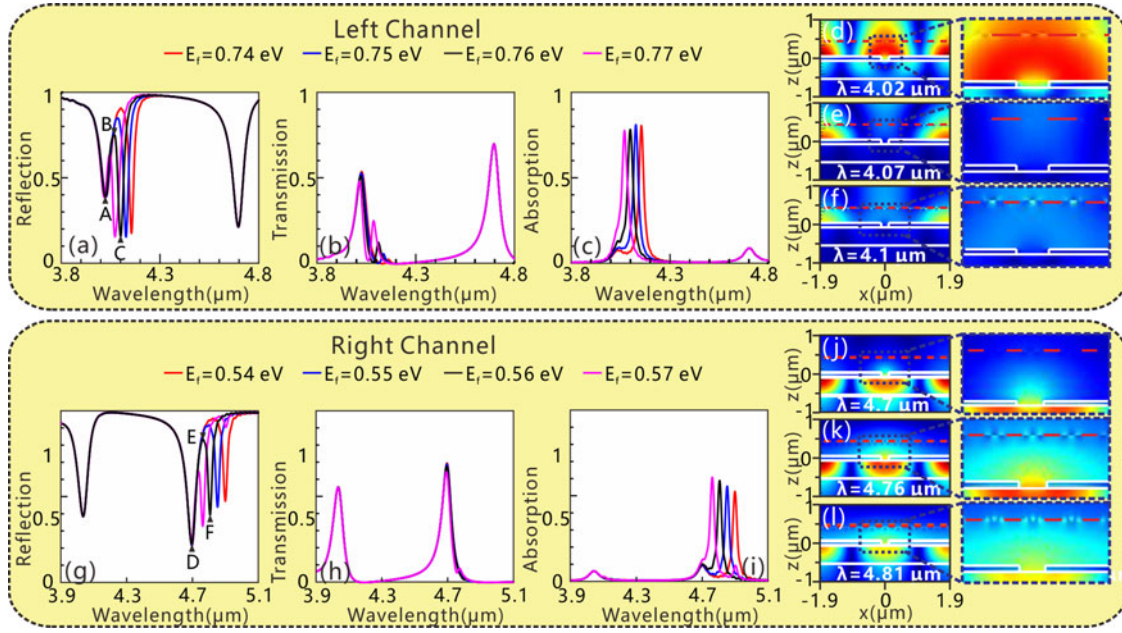
Fig. 3. Calculated reflection (a), transmission (b) and absorption (c) spectrums for the GRG with $E_f = 0.74$–0.77 eV. Spatial magnetic field distributions corresponding to reflection dips and peak represented by A (d), C (f) and B (e) in (a), respectively. Simulated reflection (g), transmission (h) and absorption (i) spectrums for the GRG with $E_f = 0.54$–0.57 eV. Spatial magnetic field distributions corresponding to reflection dips and peak represented by D (j), F (l) and E (k) in (g), respectively.

interlayer thickness d_i, the left optical channel is red-shifted obviously (up panel). Different from the results in up panel, the change of the SiN_x dielectric layer (d_s) only results in red-shift of the right optical channel (bottom channel). In addition, the influence of refractive index on all the resonant peaks are shown in Fig. 2(d). Compared with the simulated results shown in Fig. 2(c), as the refractive index of the interlayer (n_i) increases from 1.57 to 1.87, it's interesting to see that all the resonant peaks are red-shifted (up panel). While the central wavelength of the right optical channel is red-shifted when the refractive index of the SiN_x dielectric layer (n_s) increases, and that of the left optical channel is stable relatively.

When TM polarized light normally illuminates on the MGCGM structure, the simulated reflection, transmission, and absorption spectrums for the GRG with $E_f = 0.74$–0.77 eV are shown in Fig. 3(a)–(c), respectively. It is noteworthy that the Fermi levels of GRG are set to particular values under a comprehensive consideration of functional realization, feasibility and device dimension. The Fermi levels of the GRG can be further lowered by increasing the grating period. However, the reduction of Fermi levels comes at the cost of device dimension. In our simulations, the mesh size inside graphene is kept as $d_z = 0.17$ nm (2 layers for the whole graphene), which is small enough to ensure the numerical convergence. It is obvious that two reflection dips which are indicated by A and C points emerge in the reflection spectrum and the central wavelengths of those dips are 4.02 μm and 4.10 μm (black line), respectively. In addition, it is noteworthy that one reflection peak is located between the two dips distinctly, which implies that the PIT window indeed appears in the reflection spectrum. We also observe that as the Fermi levels of the GRG increases from 0.74 to 0.77 eV with a step of 0.01 eV, the amplitude of reflection

peak is increased from 0.6 to 0.9 and the central wavelength of that is red-shifted from 4.03 to 4.09 μm, respectively. Obviously, it is feasible to dynamically control the PIT effect by varying the gate voltage rather than altering the period and width of gold grating in the fabrication process. In order to get further insight into the physics mechanisms of the double reflection dips and single peak, the spatial magnetic field distributions of the reflection peak and dips indicated by A, C and B are exhibited in Fig. 3(d)–(f), respectively. As shown in Fig. 3(d), we can find that the hybrid mode consisted of cavity mode, SPPs mode and guide mode resonance is confined in the interlayer and it's stronger than that in Fig. 3(e) and (f). The reason for the excitation of the cavity mode in the interlayer can be demonstrated by the phase equation [39]

$$\varphi_{12} + \varphi_{23} + k_{MIM} d_{Au} = 2n\pi \quad n = 0, 1, \ldots N \quad (5)$$

where the phases φ_{12} and φ_{23} are caused by the reflection in the slits, and k_{MIM} is the wave vector of SPPs mode. Moreover, the excitation of the SPPs mode on the surface of gold grating is explained by the dispersion equation [39]

$$\frac{2\pi}{\lambda}\sin\theta - j\frac{2\pi}{\Lambda_m} = -\frac{2\pi}{\lambda}\sqrt{\frac{n_{Au}^2(\omega)\varepsilon_0}{n_{Au}^2(\omega) + \varepsilon_0}} = k_{spp} \quad (6)$$

where n is diffraction order, θ is the incident angle and ε is the relative permittivity of the medium closed to the surfaces of metallic grating. The extraordinary transmission shown in Fig. 3(b) has been attributed to the hybrid plasmonic mode combined with SPPs mode and cavity mode, and the excitation of cavity mode leads to strong transmission and low reflection which is represented by the reflection dip A in Fig. 3(a) [39]. Here, it should be noted that the feature of the cavity mode in

Fig. 3(d) is not very distinct to identity. The reasons for this phenomenon are as follows: (I) the hybrid plasmonic mode located around the slit consists of SPPs mode and cavity mode, and these two modes would interact with each other; (II) the thickness of the metallic grating is so small (70 nm) that the slits between the gold grating can only support the zeroth-order vertical cavity mode whose field distribution feature is not distinct to identify compared with higher-order cavity modes. Notably, the hybrid plasmonic mode has nothing to do with the Fermi levels of the GRG, therefore the central wavelengths of the reflection dip A are stable when the Fermi levels of the GRG increases from 0.74 eV to 0.77 eV. In addition, compared with the spatial magnetic field distribution of the reflection peak at 4.07 μm (Fig. 3(e)), it's interesting to see that the strong SPPs modes are excited on the graphene nanoribbons (Fig. 3(f)), and the reason for the excitation of GSPs mode is related to the resonant oscillation supported by the bound electrons of the graphene nanoribbons [31]. The excitation of the GSPs mode on the GRG can be demonstrated by the absorption spectrum in Fig. 3(c), it can be observed that pronounced absorption peaks are appeared in the absorption spectrum distinctly. Obviously, in the MGCGM structure, the diffraction excited by the gold grating can bring about the hybrid plasmonic mode with broad bandwidth. It's important to note that the resonance wavelength of the hybrid plasmonic mode excited by the gold grating is close to that of the GSPs mode on the GRG when the Fermi levels of GRG are set to 0.74–0.77 eV. Thus, we can attribute the appearance of the PIT effect in Fig. 3(a) to the destructive interference between the GSPs modes excited on the GRG and the hybrid mode in the interlayer, and it is equivalent to the case of destructive interference between two closely spaced broadened resonances decaying to the same continuum [40]. As shown in Fig. 3(e), it is the GSPs mode excited on the GRG that suppresses the hybrid plasmonic mode in the interlayer, and the intensity of the hybrid mode located next to the slit in the metallic grating becomes very weak. Notably, the formation of the PIA effect in Fig. 3(a) is similar to that of the double GRGs structure provided by Ref. [29], where the Fermi levels of two GRGs are slightly detuned to achieve the difference of the excitation wavelength between the GSPs on the two GRGs. The emerging transmission dips in Fig. 3(b) also demonstrate this inference due to the cavity mode in the slits is decayed.

It is noteworthy that the excitation wavelength of the GSPs on GRG approaches to the reflection dip around 4.71 μm when the Fermi levels of GRG are lowered to 0.54–0.57 eV. It is anticipated that the PIT effect will appear in the reflection spectrum based on the mode coupling mechanism. Here, the simulated reflection, transmission, and absorption spectrums for the GRG with $E_f = 0.54$–0.57 eV are shown in Fig. 3(g)–(i), respectively. As expected, the pronounced PIT effects emerge in the reflection spectrum, and the PIT effect can be controlled by altering the Fermi levels of GRG dynamically. The spatial magnetic field distributions of the reflection peak and dips represented by D, F and E in (g) are exhibited in Fig. 3(j)–(l), respectively. As shown in Fig. 3(j), we can find that the hybrid mode consisted of SPPs mode and guide mode resonance is confined in the SiN$_x$ dielectric waveguide layer, rather than the interlayer upon the
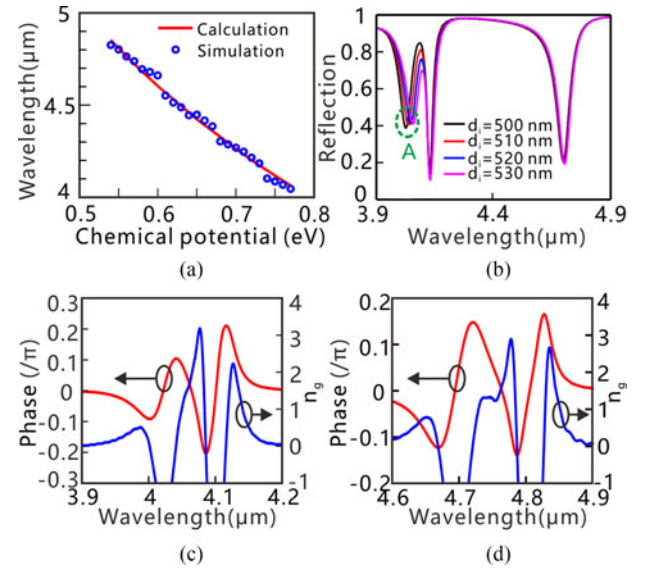

Fig. 4. (a) The simulated results (blue circles) and theoretical results (red line) for the resonant wavelength of the GSPs. (b) The reflection spectrums for different thicknesses of the interlayer. The corresponding phase shift response and group indices for proposed MGCGM structure with $E_f = 0.76$ eV (c) and $E_f = 0.56$ eV (d).

gold grating. Here, it's worth nothing that that the GRG is far from the SiN$_x$ dielectric layer and GSPs mode is highly confined on graphene, thus the GSPs mode on the GRG is not directly coupled with the hybrid mode in the SiN$_x$ dielectric layer. Obviously, the reason for the occurrence of the PIT effect in Fig. 3(g) is quite different from that in Fig. 3(a). From the magnetic field distribution shown in Fig. 3(l), we can observe that the strong GSPs modes are excited on the graphene nanoribbons, which results in the reflection dip F in Fig. 3(g). The excitation of the GSPs modes also can be demonstrated by the absorption spectrum in Fig. 3(i), it can be found that obvious absorption peaks emerge in the absorption spectrum with amplitude close to 0.60. Compared with the results in Fig. 3(i), the relatively weak GSPs modes exist on the GRG and strong hybrid mode are also confined in the SiN$_x$ dielectric layer simultaneously. As a result, it is the GSPs mode excited on the GRG that suppresses the hybrid mode equivalently due to the absorption of electromagnetic wave, leading to the occurrence of the reflection peak B in Fig. 3(g).

It should be noticed that the resonant wavelength λ_{res} of the GRG can be obtained from the quasi-static analysis [41] and be expressed as

$$\lambda_{res} \approx \frac{2\pi c\hbar}{e}\sqrt{\frac{\eta\left(n_0^2 + n_i^2\right)\varepsilon_0 w_g}{2E_F}} \tag{7}$$

where the constant $\eta = 0.45$ is a fitting parameter deduced from the simulated results, ω_g is the width of the graphene nanoribbons, and $n_0\,(=1)$ is the refractive index of air. As shown in Fig. 4(a), it is obvious that as the Fermi levels of GRG increase, the resonant wavelengths of the GSPs mode move towards the shorter wavelength region gradually. And the simulated results (blue circles) are indeed consistent with the theoretical results (red line), which also indicates that the appearances of the PIT
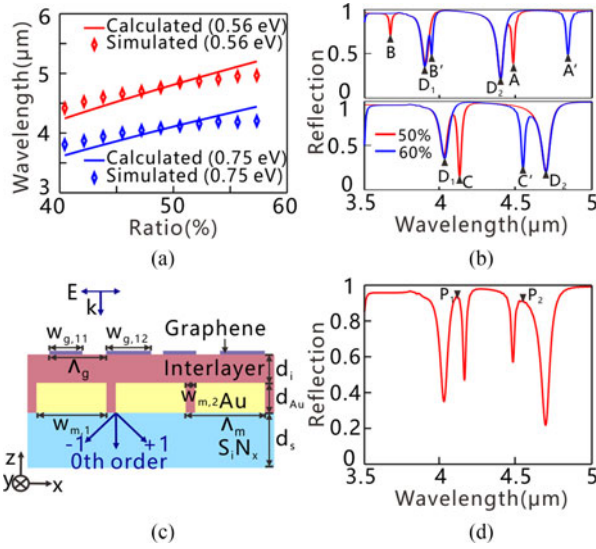
Fig. 5. (a) The simulated results (circles) and theoretical results (solid line) for the resonant wavelength of the GSPs versus different occupation ratios. (b) The reflection spectrums for different occupation ratios of the GRG when $E_f = 0.75$ eV (up panel) and 0.56 eV (bottom panel). (c) The schematic of the MGCGM structure with different occupation ratios of GRG. (d) The reflection spectrum for the occupation ratios of the adjacent GRG are 40% and 50%.

effects in Fig. 3(a) and (g) is related to the excitation of the GSPs mode. In addition, it is anticipated that the PIT effect is not only controlled by the Fermi levels of the GRG but also influenced by the thickness of the interlayer. We calculate the reflection spectrum for the MGCGM structure with different thickness of the interlayer $d_i = 500, 510, 520$ and 530 nm, and the simulated results are shown in Fig. 4(b). Here, the Fermi levels of GRG are fixed as 0.76 eV. It can be found that the central wavelengths of the GSPs mode are stable, while the amplitudes of the reflection peaks are reductive and the reflection dips represented by A are red-shifted slightly. We can attribute this phenomenon to the resonant wavelength of the hybrid mode confined in the interlayer is red-shifted when the thickness of the interlayer increases from 500 nm to 530 nm [according to (4)], while the excitation wavelength of GSPs mode is not sensitive to the thickness. Besides, the group index n_g of the designed MGCGM structure can be evaluated from the formula [42]

$$n_g = -\frac{c_0}{d_g + d_i + d_{Au} + d_s}\frac{d\varphi(\omega)}{d\omega} \qquad (8)$$

where $\varphi(\omega)$ is the reflection phase as a function of frequency ω. The corresponding phase shift and group indices for different Fermi levels of the GRG are shown in Fig. 4(c) and (d), respectively. Obviously, the maximum group index of the PIT effects with $E_f = 0.76$ eV is about 3.2, while the bandwidth of the slow light effect can almost reach 75 nm. As a result, the relatively wide-bandwidth slow light without distortion can be obtained based on the PIT effect in our proposed MGCGM structure.

Next let us proceed to consider the influence of occupation ratio (OR) on the PIT effect. According to (7), as the width of graphene ribbons increases, the resonant wavelength of GRG is red-shifted. The solid lines in Fig. 5(a) exhibit the variation

regularity of resonant wavelength when the OR of GRG increases from 40% to 60%. We can observe that the excitation wavelength of GSPs mode for $E_f = 0.75$ eV red-shifts from 3.6 μm to 4.3 μm, while that of the GSPs mode for $E_f = 0.56$ eV red-shifts from 4.2 μm to 5.2 μm. In addition, the theoretical results (solid line) are consistent with those simulated results (circles) in Fig. 5(a). (b) exhibits the simulated reflection spectrums for different ORs of the GRG when the Fermi levels of graphene ribbons are $E_f = 0.75$ eV (up panel) and 0.56 eV (bottom panel), respectively. From Fig. 5(b), as expected, the reasons for occurrence of the reflection dip D_1 and D_2 are related to the hybrid mode in the waveguide layer, thus the central wavelengths of those dips are stable for different ORs. It is also noteworthy that as the resonant wavelength of the GSPs mode red-shifts, the pronounced PIT effect emerges in the positions closed to the reflection dip D_1 and D_2. Thus, it provides a promising method to achieve multi-PIT effects in the reflection spectrum simultaneously by controlling the OR of GRG in the fabrication process. Here, we also propose a MGCGM structure with different ORs of the GRG [shown in Fig. 5(c)] to achieve multi-PIT effects. Here, the period of the GRG is fixed to be 380 nm, and the OR of adjacent periodic unit is different. Namely, the GRGs with different widths $w_{g,11}$ and $w_{g,12}$ are deposited onto the interlayer alternately. The reflection spectrum of MGCGM structure are simulated with 40% ($w_{g,11} = 152$ nm) and 50% ($w_{g,12} = 190$ nm) ORs of the adjacent GRGs. From the simulated results shown in Fig. 5(d), it can be observed that two pronounced PIT effects emerge in the reflection spectrum simultaneously, which provides a new method to realize the multi-channel filter, sensor, slow light in the mid-infrared region.

Finally, we also investigate the influence of refractive index on the reflection spectrum, which is conducible to the design of graphene refractive index sensor. It should be noticed that the GRG has been demonstrated suitable for the realization of refractive index sensor and biosensor in the mid-infrared region. The reason is that the GSPs can enhance the interaction between analyte and SPPs, and mid-IR range contains the vibration features of biomolecule [43]. In addition, compared with the refractive index sensor based on the simple optical characteristics, the refractive index sensor based on the PIT effect exhibits great potentials for sensing because the optical characteristics are steeper and the figure of merit is large [2]. Here, the simulated reflection spectrums for different refractive indices of the interlayer are exhibited in Fig. 6(a) ($E_f = 0.54$ eV) and (b) ($E_f = 0.74$ eV), respectively. It can be found that all the peaks of the PIT effects and the reflection dips originated from the GSPs are red-shifted obviously, whereas the reflection dips caused by the hybrid plasmonic mode in the waveguide layer only show negligible change. From the simulated results, we can reach a conclusion that the GSPs mode is more sensitive to the change of refractive index. Motivated by above analysis, we calculate the reflection spectrums when the analyte covers on the MGCGM structure with different refractive indices, and the simulated results are shown in Fig. 6(c) ($E_f = 0.54$ eV) and (d) ($E_f = 0.74$ eV), respectively. Here, the OR of GRG and the thickness of analyte layer are kept as 50% and 30 nm,
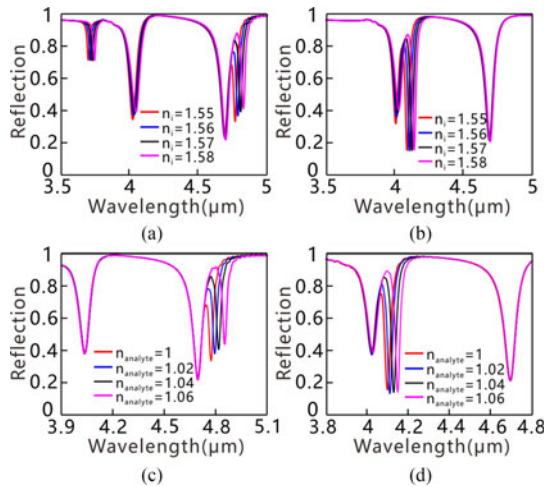
Fig. 6. Simulated reflection spectrums for different refractive indices of the interlayer with $E_f = 0.54$ eV (a) and $E_f = 0.74$ eV (b). Simulated reflection spectrums for different refractive indices of the analyte covered on the MGCGM structure with $E_f = 0.54$ eV (c) and $E_f = 0.74$ eV (d).

respectively. It can be clearly seen from the results that the central wavelength of PIT effect is red-shifted and the amplitude of the peak increases from 0.62 to 0.91 ($E_f = 0.54$ eV) when the refractive index of analyte increases from 1 to 1.06. Calculated results indicate that the sensitivity of 1150 nm/RIU (950 nm/RIU) can be obtained for the reflection peak of PIT effect in Fig. 6(c) (Fig. 6(d)).

IV. CONCLUSION

In conclusion, in this article, the tunable PIT effect is demonstrated and investigated in a MGCGM structure. The PIT effects in reflection spectrum are originated from two different mechanisms: one is based on the direct coupling between GSPs on GRG and the hybrid mode in the dielectric layer, the other is related to the absorption of graphene surface plasmons. The simulated results indicate that high tunability in amplitude and wavelength of the PIT effect can be obtained by controlling the Fermi levels of graphene ribbons. The tunable PIT effect based on the MGCGM structure our proposed has significant applications in modulators, switching, sensors, absorbers, slow light and so on, and the MGCGM structure is much easier to fabricate.

REFERENCES

[1] S. Zhang, D. A. Genov, Y. Wang, M. Liu, and X. Zhang, "Plasmon-induced transparency in metamaterials," *Phys. Rev. Lett.*, vol. 101, 2008, Art. no. 047401.

[2] S. Zhan, H. Li, Z. He, B. Li, Z. Chen, and H. Xu, "Sensing analysis based on plasmon induced transparency in nanocavity-coupled waveguide," *Opt. Express*, vol. 23, pp. 20313–20320, 2015.

[3] T. Zhang *et al.*, "Dynamically tunable plasmon induced absorption in graphene-assisted metallodielectric grating," *Opt. Express*, vol. 25, pp. 26221–26233, 2017.

[4] R. D. Kekatpure, E. S. Barnard, W. Cai, and M. L. Brongersma, "Phase-coupled plasmon-induced transparency," *Phys. Rev. Lett.*, vol. 104, 2010, Art. no. 243902.

[5] Q. Lu *et al.*, "Plasmon-induced transparency and high-performance slow light in a plasmonic single-mode and two-mode resonators coupled system," *J. Lightw. Technol.*, vol. 35, no. 9, pp. 1710–1717, May 2017.

[6] N. Liu *et al.*, "Plasmonic analogue of electromagnetically induced transparency at the Drude damping limit," *Nature Mater.*, vol. 8, pp. 758–762, 2009.

[7] W. Cao, R. Singh, C. Zhang, J. Han, M. Tonouchi, and W. Zhang, "Plasmon-induced transparency in metamaterials: Active near field coupling between bright superconducting and dark metallic mode resonators," *Appl. Phys. Lett.*, vol. 103, 2013, Art. no. 101106.

[8] J. Zhang, W. Bai, L. Cai, Y. Xu, G. Song, and Q. Gan, "Observation of ultra-narrow band plasmon induced transparency based on large-area hybrid plasmon-waveguide systems," *Appl. Phys. Lett.*, vol. 99, 2011, Art. no. 181120.

[9] Z. Chai, X. Hu, Y. Zhu, F. Zhang, H. Yang, and Q. Gong, "Low-power and ultrafast all-optical tunable plasmon-induced transparency in plasmonic nanostructures," *Appl. Phys. Lett.*, vol. 102, 2013, Art. no. 201119.

[10] Y. Zhu, X. Hu, Y. Fu, H. Yang, and Q. Gong, "Ultralow-power and ultrafast all-optical tunable plasmon-induced transparency in metamaterials at optical communication range," *Sci. Rep.*, vol. 3, 2013, Art. no. 2338.

[11] X. Yang, X. Hu, Z. Chai, C. Lu, H. Yang, and Q. Gong, "Tunable ultracompact chip-integrated multichannel filter based on plasmon-induced transparencies," *Appl. Phys. Lett.*, vol. 104, 2014, Art. no. 221114.

[12] Y. Lu, J. Y. Rhee, W. H. Jang, and Y. P. Lee, "Active manipulation of plasmonic electromagnetically-induced transparency based on magnetic plasmon resonance," *Opt. Express*, vol. 18, pp. 20912–20917, 2010.

[13] Q. H. Song *et al.*, "Liquid-metal-based metasurface for terahertz absorption material: Frequency-agile and wide-angle," *APL Mater.*, vol. 5, 2017, Art. no. 066103.

[14] Y. Shi *et al.*, "High-resolution and multi-range particle separation by microscopic vibration in an optofluidic chip," *Lab Chip*, vol. 17, pp. 2443–2450, 2017.

[15] Q. Song *et al.*, "Water-resonator-based metasurface: An ultrabroadband and near-unity absorption," *Adv. Opt. Mater.*, vol. 5, 2017, Art. no. 1601103.

[16] Y. Zhu, X. Hu, H. Yang, and Q. Gong, "On-chip plasmon-induced transparency based on plasmonic coupled nanocavities," *Sci. Rep.*, vol. 4, 2014, Art. no. 3752.

[17] X. Han, T. Wang, X. Li, B. Liu, Y. He, and J. Tang, "Ultrafast and low-power dynamically tunable plasmon-induced transparencies in compact aperture-coupled rectangular resonators," *J. Lightw. Technol.*, vol. 33, no. 14, pp. 3083–3090, Jul. 2015.

[18] X. Han, T. Wang, B. Liu, Y. He, and Y. Zhu, "Tunable triple plasmon-induced transparencies in dual T-shaped cavities side-coupled waveguide," *IEEE Photon. Technol. Lett.*, vol. 28, no. 3, pp. 347–350, Feb. 2016.

[19] Z. Chai, X. Hu, H. Yang, and Q. Gong, "All-optical tunable on-chip plasmon-induced transparency based on two surface-plasmon-polaritons absorption," *Appl. Phys. Lett.*, vol. 108, 2016, Art. no. 151104.

[20] A. Vakil and N. Engheta, "Transformation optics using graphene," *Science*, vol. 332, pp. 1291–1294, 2011.

[21] T. Zhang, L. Chen, and X. Li, "Graphene-based tunable broadband hyperlens for far-field subdiffraction imaging at mid-infrared frequencies," *Opt. Express*, vol. 21, pp. 20888–20899, 2013.

[22] P. C. Wu, N. Papasimakis, and D. P. Tsai, "Self-affine graphene metasurfaces for tunable broadband absorption," *Phys. Rev. Appl.*, vol. 6, 2016, Art. no. 044019.

[23] X. Shi *et al.*, "Plasmonic analog of electromagnetically induced transparency in nanostructure graphene," *Opt. Express*, vol. 21, pp. 28438–28443, 2013.

[24] G. Yao, F. Ling, J. Yue, Q. Luo, and J. Yao, "Dynamically tunable graphene plasmon-induced transparency in the terahertz region," *J. Lightw. Technol.*, vol. 34, no. 16, pp. 3937–3942, Aug. 2016.

[25] X. Han, T. Wang, X. Li, S. Xiao, and Y. Zhu, "Dynamically tunable plasmon induced transparency in a graphene-based nanoribbon waveguide coupled with graphene rectangular resonators structure on sapphire substrate," *Opt. Express*, vol. 23, pp. 31945–31955, 2015.

[26] L. Wang *et al.*, "Mid-infrared plasmon induced transparency in heterogeneous graphene ribbon pairs," *Opt. Express*, vol. 22, pp. 32450–32456, 2014.

[27] J. Xu *et al.*, "Flexible modulation of plasmon-induced transparency in a strongly coupled graphene grating-sheet system," *Opt. Express*, vol. 24, pp. 5784–5793, 2016.

[28] H. Yan, T. Low, F. Guinea, F. Xia, and P. Avouris, "Tunable phonon-induced transparency in bilayer graphene nanoribbons," *Nano Lett.*, vol. 14, pp. 4581–4586, 2014.

[29] C. Zeng, J. Guo, and X. Liu, "High-contrast electro-optic modulation of spatial light induced by graphene-integrated Fabry-Pérot microcavity," *Appl. Phys. Lett.*, vol. 105, 2014, Art. no. 121103.

[30] C. Zeng, Y. Cui, and X. Liu, "Tunable multiple phase-coupled plasmon-induced transparencies in graphene metamaterials," *Opt. Express*, vol. 23, pp. 545–551, 2015.

[31] W. Gao, J. Shu, C. Qiu, and Q. Xu, "Excitation of plasmonic waves in graphene by guided-mode resonances," *ACS Nano*, vol. 6, pp. 7806–7813, 2012.

[32] T. Zhang, L. Chen, B. Wang, and X. Li, "Tunable broadband plasmonic field enhancement on a graphene surface using a normal-incidence plane wave at mid-infrared frequencies," *Sci. Rep.*, vol. 5, 2015, Art. no. 11195.

[33] T. Zentgraf, S. Zhang, R. F. Oulton, and X. Zhang, "Ultranarrow coupling-induced transparency bands in hybrid plasmonic systems," *Phys. Rev. B*, vol. 80, 2009, Art. no. 195415.

[34] E. Sakat *et al.*, "Guided mode resonance in subwavelength metallodielectric free-standing grating for bandpass filtering," *Opt. Lett.*, vol. 36, pp. 3054–3056, 2011.

[35] T. Zhang, X. Yin, L. Chen, and X. Li, "Ultra-compact polarization beam splitter utilizing a graphene-based asymmetrical directional coupler," *Opt. Lett.*, vol. 41, pp. 356–359, 2016.

[36] G. W. Hanson, "Dyadic Green's functions and guided surface waves for a surface conductivity model of graphene," *J. Appl. Phys.*, vol. 103, 2008, Art. no. 064302.

[37] L. Ju *et al.*, "Graphene plasmonics for tunable terahertz metamaterials," *Nature Nanotechnol.*, vol. 6, pp. 630–634, 2011.

[38] L. Chen, G. P. Wang, Q. Gan, and F. J. Bartoli, "Trapping of surface-plasmon polaritons in a graded Bragg structure: Frequency-dependent spatially separated localization of the visible spectrum modes," *Phys. Rev. B*, vol. 80, 2009, Art. no. 161106.

[39] Y. Liang, W. Peng, R. Hu, and L. Xie, "Extraordinary optical properties in the subwavelength metallodielectric free-standing grating," *Opt. Express*, vol. 22, pp. 19484–19494, 2014.

[40] S. I. Bozhevolnyi, A. B. Evlyukhin, A. Pors, M. G. Nielsen, M. Willatzen, and O. Albrektsen, "Optical transparency by detuned electrical dipoles," *New J. Phys.*, vol. 13, 2011, Art. no. 023034.

[41] H.-S. Chu and C. How Gan, "Active plasmonic switching at mid-infrared wavelengths with graphene ribbon arrays," *Appl. Phys. Lett.*, vol. 102, 2013, Art. no. 231107.

[42] J. Song *et al.*, "Plasmon-induced transparency and dispersionless slow light in a novel metamaterial," *IEEE Photon. Technol. Lett.*, vol. 27, no. 11, pp. 1177–1180, Jun. 2015.

[43] D. Rodrigo *et al.*, "Mid-infrared plasmonic biosensing with graphene," *Science*, vol. 349, pp. 165–168, 2015.

Tian Zhang received the Ph.D. degree in optical engineering from Huazhong University of Science and Technology, Wuhan, China, in 2016.

She is currently working as a Postdoctoral Researcher in the State Key Laboratory of Information Photonics and Optical Communications, Beijing University of Posts and Telecommunications, Beijing, China. Her current research interests include graphene plasmons, integrated device, and photonic neural network.

Jian Dai received the Ph.D. degree from Beijing University of Posts and Telecommunications, Beijing, China, in 2013.

He is currently working in the State Key Laboratory of Information Photonics and Optical Communications, Beijing University of Posts and Telecommunications. His current research interests include microwave photonic signal generation and processing.

Yitang Dai received the B.Sc. and Ph.D. degrees in electronic engineering from Tsinghua University, Beijing, China, in 2002 and 2006, respectively.

He was a Postdoctoral Research Fellow in the School of Information Technology and Engineering, University of Ottawa, Ottawa, ON, Canada, and in the School of Applied and Engineering Physics, Cornell University, Ithaca, NY, USA, from June 2007 and July 2008, respectively. Since June 2010, he has been working as an Associate Professor in the State Key Laboratory of Information Photonics and Optical Communications, Beijing University of Posts and Telecommunications, Beijing. His research interests include microwave photonics, optical fiber communications, and fiber-based and integrated devices.

Yuting Fan received the Ph.D. degree from Beijing University of Posts and Telecommunications, Beijing, China, in 2015.

She is currently working as a Postdoctoral Researcher in the State Key Laboratory of Information Photonics and Optical Communications, Beijing University of Posts and Telecommunications. Her current research interests include optical communication systems and microwave photonics.

Xu Han, biography not available at the time of publication.

Jianqiang Li (S'05–M'10–SM'15) received the B.E. and Ph.D. degrees both from Beijing University of Posts and Telecommunications (BUPT), Beijing, China, in 2005 and 2009, respectively.

In July 2009, he joined Fujitsu R&D Center, Beijing, working on coherent optical communications. From June 2011 to May 2012, he was in the Department of Microtechnology and Nanoscience, Chalmers University of Technology, Sweden, as a Postdoctoral Researcher. He is currently an Associate Professor in the State Key Laboratory of Information Photonics and Optical Communications, BUPT. His research interests include optical communication systems, microwave photonics, and digital signal processing.

Feifei Yin received the B.Eng. and Ph.D. degrees in electronic engineering from Tsinghua University, Beijing, China, in 2007 and 2012, respectively.

He is currently an Associate Professor in the State Key Laboratory of Information Photonics and Optical Communications, BUPT. His current research interests include microwave photonics, radio over fiber subsystems, and their key optical components.

Yue Zhou received the B.Eng. degree in information engineering from Shanghai Jiao Tong University, Shanghai, China, in 2008, and the Ph.D. degree in optics and photonics from the University of Hong Kong, Hong Kong, in 2012.

From November 2012 to November 2014, he was with the Center for Free Electron Laser Science, Deutsches Elektronen-Synchrotron, Hamburg, Germany, as a Postdoctoral Researcher. He is currently an Associate Professor in the State Key Laboratory of Information Photonics and Optical Communications, Beijing University of Posts and Telecommunications, Beijing, China. His current research interests include microwave photonics and ultrafast optics.

Kun Xu received the Ph.D. degree in electronic engineering from Tsinghua University, Beijing, China, in 2003.

He joined Nanyang Technological University, Singapore, as a Visiting Scholar in 2004. He is currently a Professor and Deputy Director of IPOC, BUPT. His current research interests include radio over fiber and microwave photonics.